

# Properties of cage rearrangements observed near the colloidal glass transition

Eric R. Weeks<sup>\*,(1)</sup> and D. A. Weitz<sup>(2)</sup>

<sup>(1)</sup>Physics Department, Emory University, Atlanta, GA 30322

<sup>(2)</sup>Department of Physics and DEAS, Harvard University, Cambridge, MA 02138

(February 4, 2002)

We use confocal microscopy to study the motions of particles in concentrated colloidal systems. Near the glass transition, diffusive motion is inhibited, as particles spend time trapped in transient “cages” formed by neighboring particles. We measure the cage sizes and lifetimes, which respectively shrink and grow as the glass transition approaches. Cage rearrangements are more prevalent in regions with lower local concentrations and higher disorder. Neighboring rearranging particles typically move in parallel directions, although a nontrivial fraction move in anti-parallel directions, usually from pairs of particles with initial separations corresponding to the local maxima and minima of the pair correlation function  $g(r)$ , respectively.

PACS numbers: 61.43.Fs, 64.70.Pf, 82.70.Dd, 61.20.Ne

Many liquids undergo a glass transition when rapidly cooled, where their viscosity grows by orders of magnitude for only modest decreases in temperature. This drastic increase in viscosity is unaccompanied by significant structural changes; instead, the dynamics slow dramatically. Physically, this slowing of the dynamics reflects the confinement of any given particle by a “cage” formed by its neighbors; it is the rearrangement of the cage which leads to the final structural relaxation, allowing the particle to diffuse through the sample [1]. The dynamics of cages have been studied with scattering measurements, which probe a spatial and temporal average of their behavior, and with computer simulations; however, in real systems, the actual motion of the individual particles involved in cage dynamics and breakup are still poorly understood [1–9].

In this paper, we study the motion of the individual particles and their neighbors during cage breakup, and provide the first direct experimental visualization of this process. We use confocal microscopy to study the motion of colloidal particles in a dense suspension, an excellent model for the glass transition [10–12]. The rearrangement of cages involves the cooperative motion of neighboring particles [2–7], for example as shown in Fig. 1, where the most mobile particles have arrows indicating the direction of their motion. While most neighboring particles move in similar directions, a significant minority move in opposite directions, resulting in local changes in topology. We find particles moving in parallel directions typically have initial separations corresponding to local maxima of the pair correlation function  $g(r)$ , while pairs of particles moving in anti-parallel directions typ-

ically correspond to local minima of  $g(r)$ . We also find that the more mobile particles are located in regions with a lower local volume fraction, and higher disorder. These measurements provide a direct, quantitative physical picture of the nature of cage rearrangements.

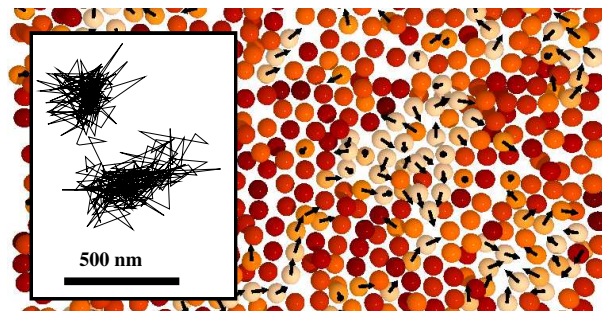


FIG. 1. Cut through a three-dimensional sample, with arrows indicating the direction of motion for particles with displacements  $\Delta r > 0.2 \mu\text{m}$ , using  $\Delta t^* = 600 \text{ s}$ . The sample has  $\phi = 0.52$ , and the cut is  $2.5 \mu\text{m}$  thick ( $\sim 1$  layer of particles). The arrows are all the same length in three dimensions, so shortened arrows indicate motion in or out of the picture. Lighter colors indicate particles with larger displacements. Inset: 120 min trajectory of one particle from this sample.

We use sterically stabilized poly-(methylmethacrylate) particles with a radius  $a = 1.18 \mu\text{m}$  [3,10,13], immersed in a mixture of decalin and cycloheptylbromide. This solvent simultaneously matches the particle index of refraction and density to mitigate the effects of scattering and sedimentation. Hard sphere particles undergo a freezing transition at a volume fraction  $\phi_f = 0.494$ , a melting transition at  $\phi_m = 0.545$ , and have a glass transition at  $\phi_g \approx 0.58$  [10,12]. To visualize the particles, we stain them with fluorescent rhodamine dye; this imparts a slight charge to the particles, shifting the phase transition boundaries to  $\phi_f \approx 0.38$ ,  $\phi_m \approx 0.42$ , and  $\phi_g \approx 0.58$ . We image a volume  $60 \mu\text{m} \times 60 \mu\text{m} \times 10 \mu\text{m}$ , containing several thousand particles, and identify particle centers with an accuracy of at least  $0.05 \mu\text{m}$  [13,14]. A typical particle trajectory is shown in the inset of Fig. 1; it exhibits caged motion, with a sudden cage rearrangement which lasts  $\sim 600 \text{ s}$ .

The effect of cages on the ensemble dynamics is well known [1–9,12] and is evident from the particle mean square displacement,  $\langle \Delta x^2 \rangle$ , shown in Fig. 2(a) for three supercooled colloidal fluids ( $\phi < \phi_g$ ). At the earliest time scales, particle motion is diffusive, as they have not moved far enough to encounter the cage formed by their

neighbors. As their displacement becomes larger, their motion is impeded by the cage, leading to the plateau in  $\langle \Delta x^2 \rangle$ . The displacement at the plateau decreases as  $\phi$  increases, reflecting the smaller cage size. Moreover, the cages become more long-lived with increasing  $\phi$ ; this presumably results from the fact that cage rearrangements involve a larger number of particles as the glass transition is approached [2–7]. The cage rearrangement itself leads to an upturn in  $\langle \Delta x^2 \rangle$  at the end of the plateau on the log-log plot; at even longer lag times, the asymptotic motion again becomes diffusive, albeit with a greatly decreased diffusion coefficient,  $D_\infty$ , as indicated by the dashed lines in Fig. 2(a).

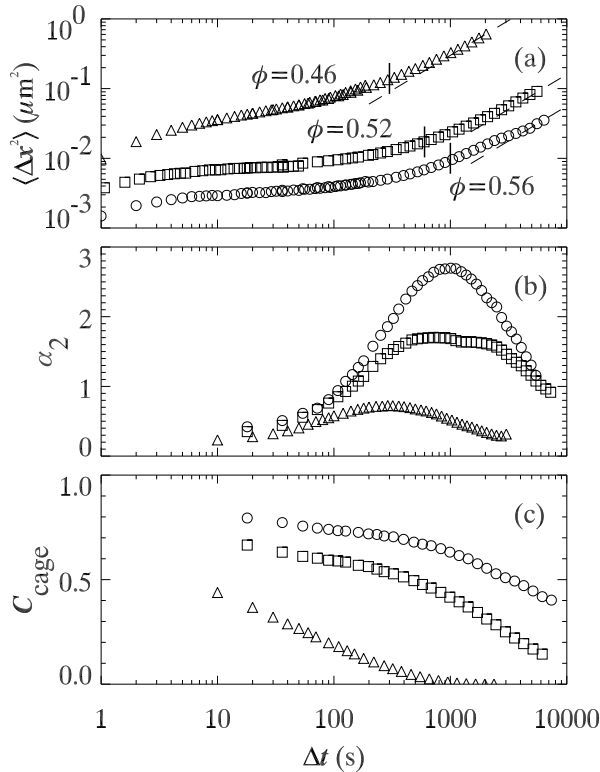


FIG. 2. (a) Mean square displacements. The diagonal straight lines indicate estimates for  $\langle \Delta x^2 \rangle \sim 2D_\infty \Delta t$ . Vertical bars indicate  $\Delta t^*$ .  $\langle \Delta x^2 \rangle$  is shown rather than  $\langle \Delta r^2 \rangle$  as the poorer  $z$ -resolution of the microscope artificially increases  $\langle \Delta r^2 \rangle$ . (b) Nongaussian parameter  $\alpha_2(\Delta t)$ . (c) The cage correlation function.

We estimate the time scale for cage rearrangement,  $\Delta t^*$ , by finding the maximum of the nongaussian parameter  $\alpha_2(\Delta t) = \langle \Delta x^4 \rangle / (3\langle \Delta x^2 \rangle) - 1$ , shown in Fig. 2(b).  $\alpha_2$  is computed from the 1D displacement distribution function  $P(\Delta x; \Delta t)$  [3–6], and is zero for a gaussian distribution, and largest when there are broad tails. To compare these distributions for different  $\phi$ , we normalize the displacements  $\Delta r$  by the average,  $\bar{r} \equiv \langle \Delta r^2 \rangle^{1/2}$ . The radial step size distribution  $P(\Delta r/\bar{r}; \Delta t^*)$  is plotted for three values of  $\phi$  in Fig. 3(a). There are more large displacements than expected for a gaussian distribution,

shown by the dashed line; moreover, as  $\phi_g$  is approached, the tails become even broader, as shown by the circles for  $\phi = 0.56$ . This reflects the anomalously large motion of the particles undergoing cage rearrangements.

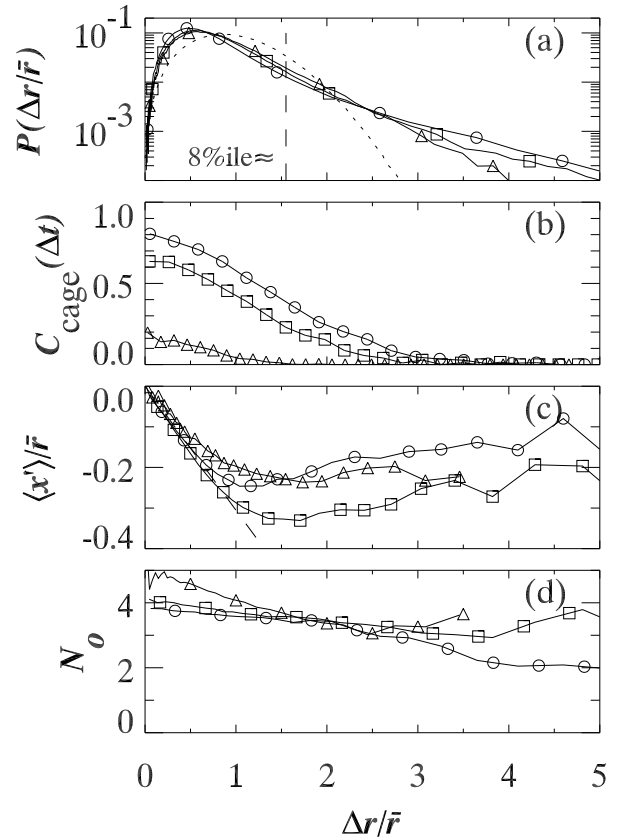


FIG. 3. (a) Step-size distribution. The vertical dashed line indicates the 8%ile cutoff. The dotted line is a gaussian with width  $\bar{r} = 1$ . (b)  $C_{\text{cage}}(\Delta t^*; \Delta r)$ . (c) Average subsequent displacement  $\langle x' \rangle$  along the direction of the original displacement  $\Delta r$ . The dashed line is a linear fit to the small  $\Delta r$  region for the  $\phi = 0.56$  data (circles). (d) The average number of ordered neighbors  $N_o$  particles have. The symbols are: triangles  $\phi = 0.46$ ,  $\Delta t^* = 300$  s,  $\bar{r} = 0.61$   $\mu\text{m}$ ; squares  $\phi = 0.52$ ,  $\Delta t^* = 600$  s,  $\bar{r} = 0.22$   $\mu\text{m}$ ; circles  $\phi = 0.56$ ,  $\Delta t^* = 1000$  s,  $\bar{r} = 0.16$   $\mu\text{m}$ .

These large displacements contribute to the increase in the mean square displacement at lag times greater than  $\Delta t^*$ . To confirm that this motion directly reflects structural relaxation, we calculate a topological cage correlation function,  $C_{\text{cage}}(\Delta t)$  [8]. We define particles as nearest neighbors if their separation is less than a cut-off distance set by the first minimum of  $g(r)$ ;  $C_{\text{cage}}(\Delta t)$  is the fraction of particles with the same neighbors at time  $t$  and time  $t + \Delta t$ , averaged over all  $t$ . As shown in Fig. 2(c), for the lowest volume fraction,  $\phi = 0.46$  (triangles), the particles are barely caged, but as  $\phi$  increases toward  $\phi_g$ , the decay of  $C_{\text{cage}}$  slows dramatically. To determine which particles are responsible for topological changes, we replot  $C_{\text{cage}}(\Delta t^*)$  as a function of the nor-

malized displacement. As shown in Fig. 3(b),  $C_{\text{cage}}(\Delta t^*)$  decreases significantly for particles with larger displacements, confirming that these particles contribute most to the structural relaxation.

To directly measure the size of the cage, we investigate the temporal correlations of the motion of individual particles [9]. Particles that remain caged must have no significant net displacement over long times; by contrast those whose cages rearrange do have net displacements. To quantify this, we compare a particle’s displacements  $\Delta\vec{r}$  and  $\Delta\vec{r}'$  during sequential time intervals of  $\Delta t^*$ . We focus on  $x'$ , the component of  $\Delta\vec{r}'$  along the direction of the original displacement  $\Delta\vec{r}$ ;  $\langle x' \rangle$  is plotted in Fig. 3(c).  $\langle x' \rangle$  is always less than zero, indicating that the average motion is anticorrelated. For small initial displacements the behavior is linear,  $x' = -c|\langle \Delta\vec{r} \rangle|$ ; larger values of  $c$  indicate more highly anticorrelated motion [9]. The cage constrains a particle so that the farther a particle moves, the farther it will move back. The linear relationship fails for larger displacements, as seen in Fig. 3(c); thus the degree of anticorrelation actually decreases – particles move shorter distances  $\langle x' \rangle$  than expected by linear extrapolation from the small  $\Delta\vec{r}$  behavior. We identify the end of the linear regime as the cage size,  $r_{\text{cage}}$  [9]. For comparison, we estimate the size of the cage by other methods. The simplest is based on the free volume of the system compared to random close packing,  $r_{\text{free}} = 4a[(\phi_{\text{rcp}}/\phi)^{1/3} - 1]$ . Another estimate comes from the mean square displacement at the cage rearrangement time scale  $\Delta t^*$ ,  $r_{\text{msd}} = \langle \Delta r^2(\Delta t^*) \rangle^{1/2}$ . The final estimate is  $\Delta r^*(\Delta t^*)$ , chosen so that 5% of particles have displacements  $\Delta r > \Delta r^*$  [3,6]. The values of these estimates are listed in Table 1 and are in good agreement. The cage size decreases as the glass transition is approached, in agreement with expectations [9,15].

We can use this cage size to model the particle motion as a random walk, alternating between steps (cage rearrangements) and pauses (caging). At long times, the diffusive motion reflects particles undergoing many steps of size  $r_{\text{cage}}$  in random directions. From the Central Limit Theorem,  $D_\infty = r_{\text{cage}}^2/2\Delta t^{**}$ , where  $\Delta t^{**}$  is the mean time between steps, or the average cage lifetime [16]. The measured values of  $D_\infty$ , and the values calculated for  $\Delta t^{**}$  are listed in Table 1. We find that  $\Delta t^{**}$  is significantly larger than  $\Delta t^*$ , the time scale for a particle to move *during* one cage rearrangement. Both grow as  $\phi$  increases, consistent with previous experiments [1,11,12] and simulations [4–9,15,6]. While the cage size decreases, it remains finite as  $\phi_g$  is approached, implying that the dramatic decrease in  $D_\infty$  is due primarily to the increasing cage lifetime. Our random-walk picture also yields an unambiguous estimate of the fraction of particles involved in cage rearrangements at any given time; it is given by the ratio  $\Delta t^*/\Delta t^{**}$ . This ratio is  $\sim 8\%$  for all samples except the most dilute (for which it is 16%); it is shown by the vertical dashed line in Fig. 3(a).

Several computer simulations looked for the underlying origins of cage rearrangements, and found correla-

tions between mobile particles and their local environments [6,7,17,18]. Mobile particles tended to be in regions with higher disorder [7,17,18], lower density [7,18], and higher potential energy (and thus higher disorder) [6]. Ultimately, our colloidal samples will crystallize, and it is possible that the evolution from disorder to crystalline order drives the structural relaxation in our experiments. To investigate this possibility, we quantify the local order with an order parameter that identifies local crystalline regions from particle positions [19]. If two adjacent particles have similar orientations of their neighbors about each of them, the two particles are ordered neighbors [20]; most particles have between 2 and 4 ordered neighbors. Particles with larger displacements have fewer ordered neighbors, as shown in Fig. 3(d), in agreement with the correlation between mobility and disorder seen in simulations [6,7,17,18]. Furthermore, the mobile colloidal particles typically move to positions where their number of ordered neighbors has increased by  $\sim 1$ , suggesting a slow evolution toward crystalline structure. We emphasize, however, that crystallization occurs on time scales significantly longer than these observations; moreover, crystallization is a nucleation and growth process, with full crystalline order of the sample resulting from the growth of only a small number of nuclei. Thus, any effect of the local crystal order on the cage rearrangement may be driven more by local variations in volume fraction, rather than an evolution to the state with the lowest global energy minimum [19]. In fact, we find that the volumes of the Voronoi polyhedra associated with the mobile particles are larger on average, giving a local volume fraction as much as  $\delta\phi = O(0.03)$  lower than the mean. This suggests that the particles with smaller  $\phi$  are farther from  $\phi_g$  and thus are more likely to rearrange, in agreement with the simulations [6,7,18].

Cage rearrangement is not strictly a localized event; instead, many neighboring particles are typically involved; they often move in similar directions, as shown by the arrows in Fig. 1 [2–7]. To quantify the propensity for motion of neighboring particles in the same direction, we calculate the distribution of angles,  $P(\theta)$ , between the displacement vectors of all neighboring particles, measured at  $\Delta t^*$  to define the displacements. The probability of observing two displacement vectors forming an angle in the range  $(\theta, \theta + d\theta; \phi, \phi + d\phi)$  is given by  $P(\theta, \phi) \sin\theta d\theta d\phi$ ; in Fig. 4(a) we plot  $P(\theta, \phi)$  which, by symmetry, depends only on  $\theta$ . This function is strongly peaked at  $\theta \approx 0$ , indicating that two particles usually move in parallel directions (“strings”) [5–7], although a significant fraction of particles move in anti-parallel directions ( $\theta \approx \pi$ , “mixing regions”) [21]. When  $\theta \approx \pi$ , particles are either converging or diverging; examples of each case can be seen in Fig. 1. We find that these “mixing” pairs of particles ( $\theta > \pi/2$ ) are approximately twice as likely to result in the two particles no longer being neighbors (compared to the pairs with  $\theta < \pi/2$ ). Thus, these rearrangements, while less frequent, are responsible for much of the topological changes.

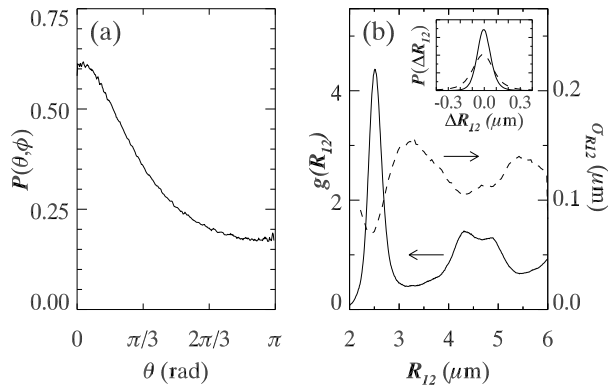


FIG. 4. (a) Probability distribution of angle between displacement vectors for two neighboring particles, as a function of the polar angle  $\theta$ . (b) Pair correlation function  $g(R_{12})$  (solid line) and width  $\sigma_{R_{12}}$  of probability distribution function  $P(\Delta R_{12}|R_{12})$  (dashed line). Inset shows  $P(\Delta R_{12}|R_{12})$  for nearest neighbors, with initial separations of  $2.4 \mu\text{m} < R_{12} < 2.6 \mu\text{m}$  (solid line), and anti-neighbors with  $3.0 \mu\text{m} < R_{12} < 3.2 \mu\text{m}$  (dotted line). All data are for  $\phi = 0.56$  and  $\Delta t^* = 1000s$ .

To investigate the nature of the correlated motion of neighboring particles, we calculate the probability distribution function,  $P(\Delta R_{12}|R_{12})$ , which measures the change in separation,  $\Delta R_{12}$ , between two nearby particles, initially separated by  $R_{12}$ , after a time interval  $\Delta t^*$ . These distributions are narrower if  $R_{12}$  corresponds to a peak of the pair correlation function,  $g(R_{12})$ , than if  $R_{12}$  corresponds to a minimum, as shown by the solid and dashed lines in the inset of Fig. 4(b), respectively. This is shown more dramatically in Fig. 4(b), where we compare the widths of the distribution functions,  $\sigma_{R_{12}}$ , directly with  $g(R_{12})$ , showing that they are anticorrelated. This is reminiscent of the behavior of the collective diffusion coefficient, which varies as the inverse of the static structure factor,  $D(q) \sim 1/S(q)$  [22]. The relaxation of fluctuations at the peak of the structure factor, which reflects the most favorable structure, is slowed relative to other values of  $q$ . Our results show a similar behavior occurs in real space; particles whose separation corresponds to a peak in  $g(R_{12})$  are in more favorable relative positions and tend to move together, so that their separation does not change; by contrast, particles whose separation corresponds to minima of  $g(R_{12})$  are in less favorable relative positions, and tend to move in antiparallel directions.

This work reveals a physical picture of cage-trapping and rearrangement. Cage rearrangements involve localized clusters of particles with large displacements, in regions with higher disorder and higher free volume. Rearranging particles typically move in parallel directions (“strings”). However, there are also “mixing regions” where particles move in other directions [Fig. 4(a)], accounting for a significant fraction of the topological rearrangements. Both the collective nature of the relaxation, and the local origin of the cage rearrangements, clearly play a key role in the behavior of supercooled fluids of

colloidal suspensions; it remains to be seen whether they also are important effects in other glasses.

We thank J. Conrad, J. C. Crocker, B. Doliwa, U. Gasser, S. C. Glotzer, H. Gould, and K. Vollmayr-Lee for helpful discussions. We thank A. Schofield for providing our colloidal samples. This work was supported by NSF (DMR-9971432) and NASA (NAG3-2284).

\* Electronic mail: weeks@physics.emory.edu

- [1] C. A. Angell, *Science* **267**, 1924 (1995); F. H. Stillinger, *ibid.* **267**, 1935 (1995); M. D. Ediger, C. A. Angell, S. R. Nagel, *J. Phys. Chem.* **100**, 13200 (1996); C. A. Angell, *J. Phys. Cond. Mat.* **12**, 6463 (2000).
- [2] W. K. Kegel and A. van Blaaderen, *Science* **387**, 290 (2000).
- [3] E. R. Weeks, J. C. Crocker, A. C. Levitt, A. Schofield, D. A. Weitz, *Science* **287**, 627 (2000).
- [4] W. Kob, C. Donati, S. J. Plimpton, P. H. Poole, S. C. Glotzer, *Phys. Rev. Lett.* **79**, 2827 (1997).
- [5] C. Donati et al., *Phys. Rev. Lett.* **80**, 2338 (1998).
- [6] C. Donati, S. C. Glotzer, P. H. Poole, W. Kob, S. J. Plimpton, *Phys. Rev. E* **60**, 3107 (1999).
- [7] D. N. Perera and P. Harrowell, *J. Chem. Phys.* **111**, 5441 (1999).
- [8] E. Rabani, J. D. Gezelter, and B. J. Berne, *J. Chem. Phys.* **107**, 6867 (1997).
- [9] B. Doliwa and A. Heuer, *Phys. Rev. Lett.* **80**, 4915 (1998).
- [10] P. N. Pusey and W. van Meegen, *Nature* **320**, 340 (1986).
- [11] E. Bartsch, V. Frenz, S. Möller, H. Silesco, *Physica A* **201**, 363 (1993).
- [12] W. van Meegen and S. M. Underwood, *Phys. Rev. E* **49**, 4206 (1994).
- [13] A. D. Dinsmore, E. R. Weeks, V. Prasad, A. C. Levitt, D. A. Weitz, *Appl. Optics* **40**, 4152 (2001).
- [14] J. C. Crocker and D. G. Grier, *J. Colloid Interface Sci.* **179**, 298 (1996).
- [15] P. Allegrini, J. F. Douglas, and S. C. Glotzer, *Phys. Rev. E* **60**, 5714 (1999).
- [16] E. R. Weeks and H. L. Swinney, *Phys. Rev. E* **57**, 4915 (1998).
- [17] H. Yin and B. Chakraborty, *Phys. Rev. Lett.* **86**, 2058 (2001).
- [18] V. A. Luchnikov, N. N. Medvedev, Yu. I. Naberukhin, V. N. Novikov, *Phys. Rev. B* **51**, 15569 (1995).
- [19] P. Rein ten Wolde, M. J. Ruiz-Montero, D. Frenkel, *J. Chem. Phys.* **104**, 9932 (1996); U. Gasser, E. R. Weeks, A. Schofield, P. N. Pusey, D. A. Weitz, *Science* **292**, 258 (2001).
- [20] The normalized order parameter  $\hat{\mathbf{q}}_l(i)$  of particle  $i$  has  $(2l + 1)$  complex components

$$\hat{q}_{lm}(i) = \frac{C}{B(i)} \sum_{j=1}^{B(i)} Y_{lm}(\hat{\mathbf{r}}_{ij}), \quad (1)$$

where  $B(i)$  is the number of nearest neighbors of particle  $i$ ,  $C$  is a normalization factor such that  $\sum_m \hat{q}_{lm}(i) \hat{q}_{lm}^*(i) = 1$ ,  $\hat{r}_{ij}$  is the unit vector pointing from particle  $i$  to its neighbor  $j$ , and  $Y_{lm}$  is a spherical harmonic function. Neighboring particles  $i$  and  $j$  are ordered neighbors if  $|\sum_m \hat{q}_{lm}(i) \hat{q}_{lm}^*(j)|$  exceeds a threshold value of 0.5. As in other studies [19], we used  $l = 6$ .

- [21] The distribution  $P(\theta, \phi)$  remains qualitatively unchanged even considering only pairs of particles with large displacements, which are involved in cage rearrangements.
- [22] P. N. Pusey, in *Liquids, Freezing and the Glass Transition*, edited by J. P. Hansen, D. Levesque, and J. Zinn-Justin (Elsevier, Amsterdam, 1991), Chap. 10.

TABLE I. Estimates for the cage size, the cage rearrangement time scale  $\Delta t^*$ , the cage lifetime  $\Delta t^{**}$ , and the asymptotic diffusion coefficient  $D_\infty$ .

$\phi$	cage size ( $\mu\text{m}$ )				time scales (hr)		$D_\infty$ ( $\mu\text{m}^2/\text{s}$ )
	$r_{\text{cage}}$	$r_{\text{free}}$	$r_{\text{msd}}$	$\Delta r^*$	$\Delta t^*$	$\Delta t^{**}$	
0.46	0.75	0.55	0.63	1.12	0.083	0.52	$15 \cdot 10^{-5}$
0.52	0.35	0.35	0.23	0.40	0.17	2.1	$0.80 \cdot 10^{-5}$
0.53	0.45	0.31	0.27	0.49	0.67	9.4	$0.30 \cdot 10^{-5}$
0.56	0.25	0.21	0.17	0.29	0.28	3.3	$0.26 \cdot 10^{-5}$